Ion velocity effect governs damage annealing process in defective $KTaO_3$

G. Velişa[a*], D. Iancu[a], E. Zarkadoula[b**], Y. Tong[c], Y. Zhang[d,e], W.J. Weber[d***]

[a]Horia Hulubei National Institute for Physics and Nuclear Engineering, Măgurele, IF 077125, Romania

[b]Center for Nanophase Materials Sciences, Oak Ridge National Laboratory, Oak Ridge, TN 37831, USA

[c]Institute for Advanced Studies in Precision Materials, Yantai University, Yantai, Shandong 264005, China

[d]Department of Materials Science & Engineering, University of Tennessee, Knoxville, TN 37996, USA

[e]Energy and Environment Science & Technology, Idaho National Laboratory, Idaho Falls, ID 83415, USA

Abstract

Effects of electronic to nuclear energy losses (S_e/S_n) ratio on damage evolution in defective $KTaO_3$ have been investigated by irradiating pre-damaged single crystal $KTaO_3$ with intermediate energy O ions (6 MeV, 8 MeV and 12 MeV) at 300 K. By exploring these processes in pre-damaged $KTaO_3$ containing a fractional disorder level of 0.35, the results demonstrate the occurrence of a precursory stage of damage production before the onset of damage annealing process in defective $KTaO_3$ that decreases with O ion energy. The observed ionization-induced annealing process by ion channeling analysis has been further mirrored by high resolution transmission electron microscopy analysis. In addition, the reduction of disorder level is accompanied by the broadening of the disorder profiles to greater depth with increasing ion fluence, and enhanced migration is observed with decreasing O ion energy. Since S_e (~ 3.0 keV nm^{-1}) is nearly constant for all 3 ion energies across the pre-damaged depth, the difference in behavior is due to the so-called "*velocity effect*": the lower ion velocity below the Bragg peak yields a confined spread of the electron cascade and hence an increased energy deposition density. The inelastic thermal spike calculation has further confirmed the existence of a velocity effect, not previously reported in $KTaO_3$ or very scarcely reported in other materials for which the existence of ionization-induced annealing has been reported. In other words, understanding of ionization-induced annealing has been advanced by pointing out that ion velocity effect governs the healing of pre-existing defects, which may have significant implication for the creation of new functionalities in $KTaO_3$ through atomic-level control of microstructural modifications, but may not be limited to $KTaO_3$.

Keywords: $KTaO_3$; defect analyses; defects simulation; HTEM; velocity effect.

* Corresponding author. Horia Hulubei National Institute for Physics and Nuclear Engineering, Măgurele, IF 077125, Romania
E-mail addresses: gihan.velisa@nipne.ro (Gihan Velişa), Tel: +4 0723-933-922
** Corresponding author. Center for Nanophase Materials Sciences, Oak Ridge National Laboratory, Oak Ridge, TN 37831, USA.
E-mail addresses: zarkadoulae@ornl.gov (Eva Zarkadoula)
*** Corresponding author. Materials Science and Engineering, University of Tennessee, Knoxville, TN 37006, USA.
E-mail addresses: wjweber@utk.edu (William J. Weber), Tel: +1 865-974-0415

1. Introduction

Scientific and industrial interest in ion beam modification of potassium tantalate ($KTaO_3$) properties has rapidly exploded in the last decade, ignited by the tunability of its optical [1–3] and electronic [4–6] properties through irradiation-induced defects [7], which makes $KTaO_3$ suitable for future optoelectronic and spintronic applications [7,8]. All these applications require effective control of the structural modification, but this is an extremely difficult task, since it demands in-depth knowledge of the interactions of ions with the local defect states in the corresponding material and the resulting evolution of radiation damage [9–11]. As a consequence, several studies have focused on understanding the response of pristine (undamaged) $KTaO_3$ to irradiation with either low-energy ions ($E \leq 1$ keV/amu) or high-energy ions ($E > 1$ MeV/amu). In general, the response of insulators, semiconductors and metals to ion irradiation is dependent on the partitioning the energy loss of ions to electrons and target atoms at low and high energy regimes as a variant parameter, and $KTaO_3$ does not deviate from this generally accepted behavior. It is well established that the energy loss of ions varies significantly with energy and can be decomposed between energy transferred to target atoms via elastic interactions and the energy transferred to electrons via inelastic interactions [12,13]. The former and latter processes are known as nuclear energy loss (S_n) and electronic energy loss (S_e), respectively.

In crystalline $KTaO_3$, ion irradiation with low-energy ion results in amorphization of the implanted layer at a given ion fluence (or dose), through a defect-stimulated mechanism [12], and the corresponding critical ion fluence necessary for amorphization shifts to higher values with increasing irradiation temperature [13,14]. The response of pristine crystalline $KTaO_3$ to high-energy ion irradiations has also been the subject of several investigations [8,15,16], and these lead to the conclusion that pristine $KTaO_3$ is relatively sensitive to swift heavy ions (SHI) irradiations ($E > 1$ MeV/amu) and undergoes discontinuous to continuous amorphous ion track formation with increasing ion energy or electronic energy loss. Discontinuous amorphous track formation in $KTaO_3$ occurs for $S_e > 11$ keV nm^{-1} [15,16], while continuous ion tracks are observed at much higher S_e values ($S_e > 23$ keV nm^{-1}) [8,16]. Since the electronic conductivity and optical properties of these ion tracks differ significantly from the corresponding bulk material, the utilization of such differences enables the fabrication of durable field emission cathodes [17] and waveguides [18], respectively.

Introducing a pre-damaged state in $KTaO_3$ leads to significant reductions in threshold S_e values (S_e^{th}) for ion track formation and moreover, the corresponding S_e^{th} shifts to lower values with increasing pre-existing disorder, i.e., S_e^{th} decreases to 4.83 keV nm^{-1} for pre-existing defects with a maximum initial disorder fraction f_0 of 0.3 in $KTaO_3$ [19], from 6.68 keV nm^{-1} for f_0 ~0.08 [16]. Lower S_e^{th} values promote the use of small and medium particle accelerator facilities, which do not have severe limitations in terms of portability and flexibility, such in the case of large accelerator facilities. To get a deeper insight into the interactions between pre-existing defects and ionizing particles, we have also investigated the consequences of ionizing particles on damage evolution in pre-damaged $KTaO_3$ using ions with S_e values below the previously determined S_e^{th} for ion track production in defective $KTaO_3$, which clearly revealed a transition from irradiation-induced disorder production to ionization-induced damage recovery processes under 5 MeV C ions and 12 MeV O ions irradiation [19]. The initial slight increase in disorder (irradiation-induced disorder production) was tentatively attributed to in-cascade damage production induced by S_n due to the low S_e/S_n ratio; however, we stated that further work was needed to identify the specific in-cascade damage production-related processes. Having that in mind, the primary purpose of the present study was to investigate the effects of electronic to nuclear energy loss (S_e/S_n) ratio on pre-existing defects evolution in $KTaO_3$. O ion irradiation at room temperature is utilized to reveal the damage production - annealing processes. In order to keep a constant nominal value of S_e (3.0 keV nm^{-1}), as well as manage the value of S_n in order to control variations in the ratio of S_e/S_n, the irradiations were performed with O ions at three different energies: 6, 8 and 12 MeV. In addition, the O ion energies used in the current study are distributed on both sides of the S_e peak, making them suitable for studying the velocity effect on the ionization-induced annealing. This study reveals the occurrence of a precursory stage of damage production before the onset of damage annealing process in defective $KTaO_3$ with decreasing O ion energy, as well as a possible ion velocity effect in the damage annealing. As consequence of the so-called velocity effect, the S_e is confined to a smaller volume in case of the low velocity ions leading to a higher energy density. Therefore, for equal values of S_e, enhanced ionization-induced annealing process is expected for the smaller ion velocity/energy (i.e., 6 MeV O). This velocity effect has to be taken into account for the interpretation of the experimental results presented in this study.

2. Irradiation and characterization details

Three epi-polished, <100>-orientated $KTaO_3$ single crystal wafers, approximately 10 × 10 × 0.5 mm^3 in size, were obtained commercially (https://www.alineason.com/) for this study. These three wafers were simultaneously irradiated with 2.0 MeV Au ions to an ion fluence of 0.11 ions nm^{-2} (or 0.1 displacements per atom (dpa) at damage peak) in order to create a pre-damaged state with an initial maximum level of fractional disorder (f_0) of about 0.35 on the Ta sublattice. These pre-damaged samples were sequentially irradiated at 300 K with 6 MeV, 8 MeV or 12 MeV O ions. For each ion energy, a pristine sample was simultaneously irradiated with O ions for reference. Prior to and after each incremental irradiation step, Rutherford backscattering spectrometry in channeling geometry (RBS/C) was conducted, using 2.0 MeV He particles and a backscattering angle of 155°, to assess the effects of each irradiation at different ion velocities on pre-existing defect evolution in $KTaO_3$. All irradiations were carried out at 7° off the main channeling direction (i.e., <100>) to hinder ion channeling effects. Both irradiations and RBS/C measurements were performed at room temperature (~ 300 K) using the 3 MV Tandetron Cockcroft-Walton accelerator located at IFIN-HH, Magurele, Romania [20,21].

The S_e and S_n values of the ions were determined *via* the Stopping and Range of Ions in Matter (SRIM- v2006.02) code [22], using the density provided by the manufacturer (7.03 g/cm3), and these values are given in Table 1. According to SRIM calculations, the S_e values for 6 MeV, 8 MeV and 12 MeV O ions are nearly constant, with of value slightly above ~ 3.0 keV nm^{-1} within the pre-damaged layer (< 500 nm); on the other hand, the S_n values increase with decreasing ion energy. As a result, the S_e/S_n ratio at the Au-induced damage peak increases with ion energy. Here it is worth noting that the O ion energies used in the current study are distributed on both sides of the S_e peak. For example, 6 MeV O is considered in the low velocity regime (i.e., below the peak in S_e); 8 MeV is near or at the peak; and 12 MeV O is considered in the high velocity regime (i.e., above the peak in S_e). By choosing these ion energies, it is possible to explore the ion velocity effect on pre-existing defect evolution in $KTaO_3$. The local dose at the damage peak in dpa were calculated using the sum of the SRIM-generated K, Ta, and O vacancies and replacement collisions profiles for a given dose, normalized to an atomic density of $KTaO_3$ (7.896×10^{22} atoms cm^{-3}). Here one should note that the corresponding dpa value at the Au-induced damage peak (160 nm) is about 0.1 dpa, while for the highest O fluences (25.0 ions nm^{-2}) used in the current study, the corresponding dpa value at the same depth are about 0.016, 0.031, and 0. 042 dpa for 12 MeV, 8 MeV and 6 MeV O ions, respectively.

Table 1: SRIM-depicted S_n (keV nm^{-1}), S_e (keV nm^{-1}), and ratio S_e/S_n at the Au-induced damage peak (~ 160 nm) in $KTaO_3$ for indicated ion species. The local dose (dpa) at the Au-induced damage peak (~ 160 nm) for the indicated ion fluence and specific energy, *E (*MeV/u*),*

are also included. In addition, the dpa peak position, $Peak_{dpa}$ (μm), predicted by the SRIM calculations is also included.

Ion/energy	$Peak_{dpa}$ (μm)	S_n (keV nm^{-1})	S_e (keV nm^{-1})	S_e/S_n	dpa	E (MeV/u)
6 MeV ^{16}O	2.84	0.009	3.06	340	0.042 (25.0 ions nm^{-2})	0.375
8 MeV ^{16}O	3.48	0.008	3.10	387.5	0.031 (25.0 ions nm^{-2})	0.5
12 MeV ^{16}O	4.80	0.003	3.03	1010	0.016 (25.0 ions nm^{-2})	0.75

A transmission electron microscope (TEM) operated at 200 V (Talos F200X G2) was utilized to study the microstructure and collect diffraction images at the damage peak. The TEM thin foils were prepared in a field-emission electron microscope (AMBER, TESCAN) equipped with a gallium-focused ion beam (FIB). The TEM samples were fabricated perpendicular to the surface of irradiated samples and thinned by FIB to electron transparency.

3. Experimental results

The RBS channeling spectra of $KTaO_3$ single crystals irradiated with Au ions to an ion fluence of 0.11 ions nm^{-2} are depicted in Fig. 1 (a)-(c), prior to and after sequential irradiation at 300 K with 6 MeV, 8 MeV and 12 MeV O ions, respectively, at the indicated O ion fluences. In Fig. 1 (a)-(c), the RBS spectra recorded "on"-axis (aligned incidence) and "off"-axis (random incidence) for unirradiated $KTaO_3$ single crystal are also included for comparison, which are considered as references for "damage-free" and amorphous levels, respectively. As shown in Fig. 1 (a)-(c), irradiation with 2.0 MeV Au ions leads to the emergence of a well-defined damage peak in the RBS/C spectra (black open circles), which is the fingerprint for the presence of uncorrelated displaced lattice atoms within the pre-damaged layer. Subsequent irradiation with either 6 MeV or 8 MeV O ions to an ion fluence of 10.0 ions nm^{-2} produces an increase in ion channeling yield (green filled triangles) over the entire damage profile. In contrast, for 12 MeV O irradiation to an ion fluence of 10.0 ions nm^{-2}, a decrease in ion channeling yield (green filled triangles in Fig. 1(c)) is observed. It should be noted that the aligned RBS yield keeps decreasing with further increase of the 12 MeV O ion fluence from 10.0 to 25.0 ions nm^{-2}, indicating the occurrence of a dynamic annealing process. Notably, for the same incremental increase in ion fluence (i.e., from 10.0 to 25.0 ions nm^{-2}), the initial trend is reversed (i.e., channeling yield decreases with increasing O ion fluence) following irradiation with either 6 or 8 MeV O ions (pink filled squares), demonstrating that the annealing process is "*switched on*". While some dynamic annealing may be occurring at the lower ion fluences, it does not become dominant until the disorder level increases under the 6 and 8 MeV O ion irradiations (i.e., to ion fluence of 10.0 ions nm^{-2}), at which time, the dynamic annealing rate exceeds the defect production rate. In other words, a competitive two-stage phase transition process occurs under 6 and 8 MeV O ion irradiations.

For a better comparison, the relative Ta damage profiles were extracted from the RBS/C spectra shown in Fig. 1 (a)-(c) using an iterative procedure, IP, (described in detail elsewhere [23]), and the corresponding disorder profiles are plotted in Fig. 2. It is known that, based on the IP procedure, the single crystal is considered amorphous if the magnitude of the relative disorder is equal to 1.0; whereas for the pristine crystal (undamaged), it is *a priori* considered to be 0.0. In very good accordance with previous experimental studies, irradiation at 300 K with 2.0 MeV Au ions to an ion fluence of 0.11 ions nm^{-2} has resulted in the creation of a pre-damaged layer with a maximum initial fractional disorder state (f_0) of ~0.35 on the Ta sublattice. According to previous damage accumulation curves [12], the sample with $f_0 \sim 0.35$ corresponds to the intermediate level of disorder, where interstitial point defects, interstitial clusters and some minor nanoscale amorphous domains are expected to be present within the layer irradiated with 2.0 MeV Au ions to an ion fluence of 0.11 ions nm^{-2} [16]. The occurrence of a competitive two-stage phase transition process in pre-damaged $KTaO_3$ following irradiation with either 6 or 8 MeV O ions is properly mirrored by the relative Ta disorder profiles shown in Fig. 2 (a) and (b). In other words, minor increases in relative Ta disorder are observed initially over a region of depth under 6 MeV and 8 MeV O irradiation to an ion fluence of 10 ions nm^{-2}, prior to the reduction of disorder level observed with further increases in ion fluence from 10.0 to 25.0 ions nm^{-2}. In addition to damage reduction, the relative Ta damage profiles from 6 MeV and 8 MeV O irradiations broaden and extend to greater depths due to diffusional processes. Another important feature of the actual disorder profiles is the appearance of a secondary peak (not well separated) beyond the original pre-damage peak at the highest 6 MeV O and 8 MeV O ion fluence (25 ion nm^{-2}). This feature is more pronounced for 6 MeV O irradiation compared to that observed for 8 MeV O irradiation, which may be due to the ion velocity effect (see discussion below). Another reason for the appearance of a second peak may be to the higher value of S_n and decreased S_e value at these depths, that can contribute additively to irradiation-enhanced diffusion of the pre-existing defects or additional damage formation along the O ion path. Considering that for the highest 6 MeV O fluence (25.0 ions nm^{-2}) used in the current study, the corresponding additional introduced dose at the Au-induced damage peak (160 nm) is about 0.042 dpa; consequently, the higher S_n values are considered to have a weaker effect than the ion velocity effect. At higher ion velocity (12 MeV O), the initial increase in relative Ta disorder is not observed, and only recovery occurs that does not increase substantially at the higher fluence. This peculiar behavior at higher O fluences stimulates the inception of the following hypothesis: ion velocity effect may govern damage annealing process in defective $KTaO_3$, as discussed in more detail below.

The RBS/C analyses of pristine $KTaO_3$ irradiated with all three O ion energies (see Fig. 1(d) – (f)) show significant increases in the backscattering yield compared with the ion channeling spectra recorded for unirradiated sample, even at the lowest ion fluences used in the current study (10.0 ions nm^{-2}). This indicates that measurable additional defects detected by RBS/C are generated via O ion irradiation in the near surface layer (< 450 nm) created by the 2.0 MeV Au ions irradiation. Unfortunately, it was impossible to perform meaningful RBS/C analysis on the 12 MeV O irradiated pristine $KTaO_3$ at the highest ion fluences used in the current study (25.0 ions nm^{-2}) because during the mounting/dismounting procedure for the sample, additional microcracks were induced that added to the ones already present on the surface. Cracking due to volume swelling associated with a buried amorphous layer, which is highly expected around the estimated O projected range (not the focus of this current study), may explain the initial cracks observed in the present study [16,24]. Note that the increase in rate of dechanneling yield with ion fluence is more pronounced at a given depth (or channel) under 6 MeV O ion irradiation (Fig. 1 (d)) than under 8 MeV O ion irradiation (Fig. 1 (e)). This indicates that the rate of disordering in pristine $KTaO_3$ is higher for 6 MeV O ions than would be expected for 12 MeV O ions at the same high fluence. Note that the slight upturn in yield at channel numbers 400 to 430 for 6 MeV O (see arrow in Fig. 1 (d)) may be due to approaching the peak in damage production, which is shallower than in the case of 8 MeV or 12 MeV O ions.

In order to accurately evaluate the irradiation-induced fractional disorder in pristine $KTaO_3$ due to O ions irradiations, the ratio, *r,* of the relative backscattering yield to the amorphous level was calculated utilizing the following expression [16,25]: $r = (\chi_d - \chi_p) / (\chi_a - \chi_p)$, where χ_d, χ_p and χ_a are the backscattering yields at given channel (or depth) in the pristine reference sample without ion irradiation and in amorphous $KTaO_3$, respectively. The resulting disorder (r) levels on the Ta lattice for the 6, 8, and 12 MeV O ion irradiations are plotted in Fig. 3. The general trend from the data shown in Fig. 3 (a) is that the total Ta-lattice disorder increases with decreasing O ion energy, as demonstrated by the data corresponding to a fluence of 10.0 ions nm^{-2} for each O ion energy. In other words, the near surface damage within the first 600 nm is more damaged under 6 MeV O ion irradiation than for 12 MeV O ions (see Fig. 3(a)). However, the difference in the disordering rate observed for the lowest O ion fluence, disappears at the higher fluence (see Fig. 3 (b)), as demonstrated by the data corresponding to a fluence of 25.0 ions nm^{-2} for 6 MeV and 8 MeV O ions, indicating that there may be some saturation in damage production near the surface as damage production becomes comparable to the ionization-induced dynamic annealing. This assumption is consistent with the formation of a precursory stage of damage production before the onset of damage annealing process in pre-damaged samples under 6 and 8 MeV O ion irradiations. Since discontinuous amorphous track formation in $KTaO_3$ occurs for $S_e > 11$ keV nm^{-1} [8,15,16], the formation of ion tracks in pristine $KTaO_3$ under 6 MeV O and 8 MeV O ion irradiations is not expected. Given that our ion channeling analysis has revealed a linear increase in disorder in pristine $KTaO_3$ for all incremental O ion energy used in this study, the formation of some interstitial point defects and clusters (isotropic scattering centers) is expected for 6 MeV and 8 MeV O ion irradiations.

The observed ionization-induced annealing process by RBS/C analysis has been further mirrored by high resolution transmission electron microscopy (HRTEM) analysis. Fig. 4(a) shows a HRTEM micrograph recorded at Au-induced damage peak (~160 nm) on a $KTaO_3$ single crystal irradiated with 2.0 MeV Au ions to an ion fluence of 0.11 ions nm^{-2} at 300 K. The micrograph indicates that most of the defects created during Au irradiation at the indicated ion fluence are damaged pockets surrounded by crystalline regions. The measured average size of the damage pockets is ~ 4 nm in diameter. In the case of the pre-damaged $KTaO_3$ sample and subsequently irradiated with 6 MeV O ions to an ion fluence of 25.0 ions nm^{-2} at 300 K, the HRTEM micrograph recorded at the same depth of Au-induced damage peak (see Fig. 3(b)), shows that 6 MeV O ions do anneal the pre-existing, since the contribution of the crystalline fraction dominates at the indicated O ion fluence due to the decrease in damaged fraction. This observation is consistent with the quantitative analysis of RBS/C spectra recorded on pre-damaged $KTaO_3$ prior to and after following 6 MeV O ions irradiations (Fig. 2(a)). When comparing the Fast Fourier transform (FFT) pattern of pre-damaged and healed $KTaO_3$ respectively, computed from the micrographs, it is obvious that athermal annealing of pre-existing defects in $KTaO_3$ occurs under irradiation with 6 MeV O ions to an ion fluence of 25.0 ions nm^{-2}. For example, the pronounced attenuation of diffused scattering rings from the recrystallized region as compared to the pre-damaged region (much more visible diffuse scattering rings) indicates its recrystallized character (less damaged).

To understand the effect of pre-exiting damage on the evolution of the lattice temperature, the spatial evolution of lattice temperature in pre-damage layer of $KTaO_3$ irradiated with O ions was mirrored using the inelastic thermal spike (i-TS) model. In the i-TS model, the atomic and electronic systems are treated as two coupled subsystems where energy can be exchanged between them, as described by two heat diffusion equations, one for each subsystem:

$$C_e(T_e)\frac{\partial T_e}{\partial t} = \frac{1}{r}\frac{\partial}{\partial r}\left[r\, K_e(T_e)\frac{\partial T_e}{\partial r}\right] - g(T_e - T_a) + A(r,t) \qquad (1)$$

$$C_a(T_a)\frac{\partial T_a}{\partial t} = \frac{1}{r}\frac{\partial}{\partial r}\left[r\, K_a(T_a)\frac{\partial T_a}{\partial r}\right] + g(T_e - T_a) \qquad (2)$$

Here, K_a and K_e are the thermal conductivity for the subsystems, C_a and C_e are the specific heat coefficients for the lattice and electrons, respectively, and g is the electron-phonon parameters. As discussed in detail in Refs. [26,27]the thermal conductivity K_e and specific heat coefficient C_e are 100 W m^{-1} K^{-1} and 1.0 J cm^{-3} K^{-1} and the values of K_a and C_a at room temperature, as well as the value of g for pristine and pre-damaged systems can be found in Ref. [26]. A(r,t) describes the spatial and temporal energy deposition from the incident ion (6 MeV O, 8 MeV O and 12 MeV O) to the electrons [28]. The maximum temperature profiles (at a time of 30 fs) due to the passage of 6 MeV O ions are provided in Fig. 5 (a) for both pristine material and a pre-damaged system of $KTaO_3$ containing 30% Frenkel pairs. Obviously, much higher lattice temperatures are achieved in the pre-damaged sample than in the pristine sample, demonstrating that energy transfer heats the defective lattice more than pristine lattice. Similar to the case of 6 MeV O ions irradiation, higher lattice temperatures are achieved in pre-damaged sample than in pristine sample under 12 MeV O ions, as shown in Fig. 5(b). It is noteworthy that the maximum temperature profiles triggered by the creation of pre-damaged layers are qualitatively similar for 6 MeV, 8 MeV and 12 MeV O ions (Fig. 5(c)), but show distinct increase in temperature with decreasing ion energy or velocity. The reason for this difference is that within the i-TS calculations the energy dissipates over a more confined radius with the decrease in ion velocity (lower energy).

4. Discussion

The creation of ion tracks in pristine or defective semiconductors [29,30] and ceramics [31,32] is typically characterized by their strong ion velocity-dependent nature. At low ion velocity, the energy transferred to electrons is lower and more radially confined; this leads to more efficient and radially-confined transfer of energy to lattice atoms, which results in larger track radii [9]). Although the existence of a velocity effect for thermal spike annealing is expected, such an effect has only been inferred in a recent study on SiC [33] As described above, the observed difference in damage evolution cannot rule out the existence of velocity effect in defective $KTaO_3$, which is sensitive to ionization-induced annealing under certain irradiation conditions.

For 12 MeV O, where the energy is above the Bragg peak in S_e, the results suggest that dynamic annealing due to the ionization-induced thermal spike occurs without the production of a precursory stage or defect diffusion at both fluences (see Fig. 2 (c)). Obviously, the occurrence of a S_e-induced defect diffusion from 12 MeV O ions cannot be ruled out, since there is an evidence of slight peak broadening or increase in disorder beyond the original pre-damage peak (e.g., appearance of a tiny secondary peak that it is not very pronounced such in the case of 6 MeV and 8 MeV O). Moreover, there is no increase in disorder at the lowest 12 MeV O fluence (10 ion nm^{-2}) under the ion irradiation conditions used in this study. It has been clearly demonstrated in our previous study [19] that, in contrast to the current low pre-damaged level ($f_0 \sim 0.3$), a higher pre-existing damage level ($f_0 \sim 0.8$) leads to a clear increase in disorder for the same 12 MeV O ion fluence. For this higher pre-damage level, nanoscale (or larger) amorphous domains are the dominant defect structures, and the observed increase in disorder under 12 MeV O irradiation can be attributed to an irradiation-induced increase in the fraction of amorphous material due to the presence of the higher pre-damage level, similar to the increased amorphization at higher values of S_e and lower values of pre-damage, but only in the pre-damaged region (not beyond). In other words, the damage annealing under 12 MeV O ion irradiations exhibits a competitive two-stage phase transition in pre-damaged sample containing higher levels of pre-existing damage (i.e., $f_0 \geq 0.75$), while the continuous damage annealing is restricted to samples containing lower damage level ($f_0 \sim 0.3$). In this same study, pre-damaged samples containing either low (as in this study) or high levels of pre-existing damage were also irradiated with 5 MeV C ions irradiation, for which the S_e/S_n (~542) value is almost a factor of two lower than for 12 MeV O ions (~1000), but similar to 8 MeV O ions (428), and it has also been observed that a clear increase in disorder occurs for the same ion fluence (10 ion nm^{-2}), even for the low pre-existing defect disorder ($f_0 \sim 0.3$). One should also note that for 5 MeV C ($S_n \sim 0.004$ keV nm^{-1}), S_n is slightly higher compared to 12 MeV O ($S_n \sim 0.003$ keV nm^{-1}), but smaller by a factor of 2 compared to 8 MeV O ($S_n \sim 0.008$ keV nm^{-1}).

For 8 MeV O, S_n is larger by about a factor of 2 compared to 12 MeV O, and there is an increase in disorder at the lowest fluence (see Fig. 2(b)). This increase in disorder is likely due to an increase in defect production by S_n, but only in the pre-damage region (not beyond), since there is not much evidence of peak broadening or increase in disorder beyond the original pre-damage peak at the lowest 8 MeV O ion fluence (10 ion nm^{-2}). This increase in disorder at 10.0 ions nm^{-2} is probably due to the ballistic breaking up of some pre-existing defect clusters by the nuclear scattering of the O ions, which would increase the disorder across the pre-existing peak damage. On the other hand, as the 8 MeV O ion fluence increases from 10.0 to 25.0 ions nm^{-2}, there is a pronounced increase in peak broadening and an increase in disorder and secondary peak formation beyond the original damage peak. We propose the following scenario for this behavior: the elastic energy transfer to target atoms by nuclear scattering of the O ions is both ballistically breaking up some defect clusters, creating additional point defects susceptible to ionization/thermal spike annealing and diffusion, and knocking single interstitials to deeper regions in the pre-damaged state (i.e., Ta interstitials can only be knocked deeper by O ions). At the highest fluence, the ionization/thermal spike induced recovery/diffusion is causing a decrease in disorder and a shift of some of the pre-damage to deeper depths and the surface. According to SRIM calculations, S_n is largest for 6 MeV O ions and thus, the initial increase in disorder within the pre-damage region (not beyond) at the lower fluence (10 ion nm^{-2}) may be due to the same reason as above for 8 MeV O ions. This supposition is supported by a successful representation in Fig. 3 (a) of the displacement cross section (σ_{SRIM}) determined using the following expression [12]: $\sigma_{\mathrm{SRIM}} = N^*_{displ}/N_0$, where N^*_{displ} represents the number of primary displacements produced per implanted ion and unit depth and N_0 = 7.896 ×10^{22} atoms cm^{-3} is the atomic density of $KTaO_3$. The general trend from these calculations is that the σ_{SRIM} increases with decreasing O ion energy, as demonstrated by the curves corresponding for each O ion energy. This observation further allows us to assume that in the early stage (low fluence regime ≤ 10 ions nm^{-2}) of irradiation with 6 MeV and 8 MeV O ions, S_n-induced ballistic effects dominate creating additional damage within the pre-damaged layer, because S_e dissipates more broadly causing less effective dynamic annealing. This assumption is consistent with the decrease in the difference of disordering rates in pristine samples at high and low fluences under 6 and 8 MeV ion irradiations (see Fig. 3 (b)). At the highest fluence (25 ion nm^{-2}), there is an increase in disorder at deeper depths. We suggest that part of this could be due to increased defect production at increased depths due to increasing S_n with depth; the rest may be due to ballistic knocking of interstitial defects to greater depths. The origin of the secondary peak in disorder (for both 6 MeV and 8 MeV O ions) has yet to be identified, but we speculate that this may be either related to the maximum and average recoil energy of interstitials knocked on by the incident O ions or enhanced damage migration triggered by the increase of lattice temperature once the defective layer is created. In the second stage (high fluence regime >10 ions nm^{-2}), the newly produced defects in conjunction with those pre-existing defects represent the embryonic precursors for damage annealing because the electronic energy dissipated remains spatially more localized along the O ion path (higher thermal 'spike' temperature for a longer time) within the pre-damaged layer, resulting in damage annealing via enhanced migration and recombination of defects. For 6 MeV, where its energy is smallest (energy dissipation is the most spatially confined), the results suggest that damage migration is highest among all three energies used in this study. Here, one needs to keep in mind that the temperature rise along the ion path is insufficient to induce local melt quenching (ion track formation) based on the thresholds for track formation in pre-damaged $KTaO_3$ determined previously [19]. In support of this statement, we provide another piece of evidence. The high-angle annular dark field (HAADF) image recorded on pre-damaged $KTaO_3$ sample and subsequently irradiated with 6 MeV O ions to an ion fluence of 25.0 ions nm^{-2} at 300 K (see Fig. 4 (c), confirms the absence of ion tracks; however, the HAADF shows the existence of residual damage, as indicated by RBS/C (i.e., 6 MeV O ion irradiation to a fluence of 25.0 ions nm^{-2} decreases the peak disorder level from to 0.42 to 0.29).

Furthermore, the relative areal density of damage is plotted in Fig. 6, A_2/A_0, (integrated disorder over depth) as a function of specific energy, *E*, because under current experimental conditions, the reduction of disorder level is accompanied by the broadening of the disorder profiles into greater depth with increasing ion fluence (see Fig. 2). A_0 represents the integrated disorder peak for the pre-damaged $KTaO_3$, and A_2 is the integrated disorder following the O ion irradiations to an ion fluence of 25 ion nm^{-2}. Examining this representation, it is clear that the efficiency for ionization-induced defect diffusion for a nearly constant S_e value increases with decreasing O ion energy. Moreover, the efficiency for S_e-induced defect diffusion is substantially reduced for 12 MeV O ions. Given the small variation in S_e values, more pronounced broadening (diffusion) of the disorder profiles into greater depth is measured for the smaller ion velocity/energy. In other words, this representation indicates the existence of the so-called "velocity effect" on the ionization-induced annealing, since annealing is governed by enhanced migration and recombination of defect. As a consequence of this so-called "velocity effect", the S_e is deposited into a smaller radius in case of the low velocity leading to a higher energy density and, therefore, to a more effective dynamic annealing (see below the inelastic thermal spike calculation).

It is also worthwhile to compare the evolution of the lattice temperature in pre-damaged $KTaO_3$ for all incremental O ion energy used in this study (see Fig. 5(c)). Despite that the average energy loss by the incident ions via inelastic electronic excitation is similar for all incremental O ion energy used in this study (~3.0 keV nm^{-1}), the lattice temperature is decreasing with increasing ion energy (or specific energy). As stated at the end of Sect. 2, the O ion energies used in the current study are distributed on both sides of the S_e peak. This indicates that for the nearly same S_e value, the energy deposited to electrons at a higher ion velocity is dissipated over a slightly larger radius, leading to less energy/atom transferred to the lattice (lower thermal 'spike' temperatures) and consequently less efficient thermal spike annealing. Although the difference in velocities is small (see specific energy values in Table 1), all these findings support the crucial role of velocity effects in thermal spike annealing process, as was found very recently for SiC [33]. Finally, while the velocity effect on thermal spike annealing process is in an exploration stage, these findings should prompt further *in-situ* TEM analysis in conjunction with modeling and simulations to advance the fundamental understanding and develop predictive models of athermal ionization-induced annealing.

5. Summary

We have studied the electronic to nuclear energy loss (S_e/S_n) ratio effects on damage evolution in defective $KTaO_3$ by irradiating pre-damaged single crystal $KTaO_3$ with intermediate energy ions (6 MeV, 8 MeV and 12 MeV O ions) at 300 K. Our ion channeling analysis reveals a precursory stage of damage production before the onset of damage annealing process in defective $KTaO_3$ with decreasing O ion energy. It has been assumed that in the first stage (low ion fluence ≤ 10 ion nm^{-2}) of irradiation with 6 MeV and 8 MeV O ions, S_e dissipates more broadly leading to less effective dynamic annealing. Instead, S_n produces additional damage within the pre-damaged layer. In the second stage (high ion fluence > 10 ion nm^{-2}), dissipation of S_e is more localized (due to increased damage during the 1st stage that increases electron-phonon coupling) that results in more localized heat within pre-damaged layer (higher thermal ‘spike’ temperature and duration) and, in turn, promotes defect recombination or athermal annealing processes. The inelastic thermal spike calculations have shown that for the same value of S_e, the highest lattice temperature in pre-damaged $KTaO_3$ containing 30% Frenkel pairs is for the lowest ion energy (or velocity). The above-mentioned results clearly demonstrate that the target volume in which S_e is deposited substantially depends on the maximum energy transfer to electrons that decreases with the ion velocity, which, in turn, governs damage annealing process in defective $KTaO_3$. Finally, these findings underscore the importance of a comprehensive understanding of the velocity effect on the energy transfer to electrons, which is needed for predictive device processing using ion beams and to develop models of materials performance under specific radiation environments where ionization and defect production occur simultaneously.

Acknowledgments

This work was supported by a grant of the Romanian Ministry of Education and Research, CNCS—UEFISCDI, project number PN-III-P4- IDPCE2020- 1379, within PNCDI III. Experiments were carried out at 3 MV Tandetron™ accelerator from "Horia Hulubei" National Institute for Physics and Nuclear Engineering (IFIN-HH) and were supported by the Romanian Government Programme through the National Programme for Infrastructure of National Interest (IOSIN). The contributions of D. Iancu and G. Velişa to this work were also supported by the Research Programme Partnership in Priority Areas PNII MEN-UEFISCDI, contract PN 23210201. Y. Zhang was supported as part of the Laboratory Directed Research and Development Program at Idaho National Laboratory under the Department of Energy (DOE) Idaho Operations Office (an agency of the U.S. Government) Contract DE-AC07-05ID145142. The contribution of W. J. Weber was supported by the National Science Foundation under Grant No. DMR-2104228. EZ (theory and simulation works) was supported by the Center for Nanophase Materials Sciences, (CNMS), which is a US Department of Energy, Office of Science User Facility at Oak Ridge National Laboratory. Y.T. gratefully acknowledges the financial support by the National Natural Science Foundation of China (Grant No. 52001272, 52371164), Taishan Scholars Program of Shandong Province (tsqn202103052), Yantai city matching fund for Taishan Scholars Program of Shandong Province.

CRediT authorship contribution statement:

G. Velişa: Conceptualization, Visualization, Methodology, Validation, Writing–review & editing, Funding acquisition, Resources, Project administration. **D. Iancu:** Investigation, Methodology. **E. Zarkadoula:** Investigation, Resources, Writing–review & editing. **Y. Tong:** Investigation, Resources, Writing – original draft. **Y. Zhang:** Visualization, Writing –review & editing. **William J. Weber:** Visualization, Writing–review & editing, Project administration.

Conflicts of interest or competing interests: The authors declare that they have no known competing financial interests or personal relationships that could have appeared to influence the work reported in this paper.

Data and code availability: The data that support the findings of this study are available from the corresponding authors upon reasonable request.

References

[1] Laguta V V., Glinchuk M D, Bykov I P, Cremona A, Galinetto P, Giulotto E, Jastrabik L and Rosa J 2003 Light-induced defects in KTaO3 *J Appl Phys* **93** 6056

[2] Liu Y, Han X, Huang Q, Crespillo M L, Liu P, Zarkadoula E and Wang X 2021 Structural damage response of lanthanum and yttrium aluminate crystals to nuclear collisions and electronic excitation: Threshold assessment of irradiation damage *J Mater Sci Technol* **90** 95–107

[3] Wong J Y C, Zhang L, Kakarantzas G, Townsend P D, Chandler P J and Boatner L A 1992 Ion-implanted optical waveguides in KTaO3 *J Appl Phys* **71** 49–52

[4] Harashima S, Bell C, Kim M, Yajima T, Hikita Y and Hwang H Y 2013 Coexistence of two-dimensional and three-dimensional Shubnikov–de Haas oscillations in Ar + -irradiated KTaO 3 *Phys Rev B* **88** 085102

[5] Tomar R, Wadehra N, Kumar S, Venkatesan A, Sarma D D, Maryenko D and Chakraverty S 2019 Defects, conductivity and photoconductivity in Ar+ bombarded KTaO 3 *J Appl Phys* **126** 035303

[6] Ojha S K, Gogoi S K, Mandal P, Kaushik S D, Freeland J W, Jain M and Middey S 2021 Oxygen vacancy induced electronic structure modification of KTaO3 *Phys Rev B* **103** 085120

[7] Gupta A, Silotia H, Kumari A, Dumen M, Goyal S, Tomar R, Wadehra N, Ayyub P and Chakraverty S 2022 KTaO3—The New Kid on the Spintronics Block *Advanced Materials* 2106481

[8] Han X, Zarkadoula E, Huang Q, Crespillo M L, Liu C, Zhang M, Wang X and Liu P 2022 Nanostructures evolution assessment and spectroscopic properties modification induced by electronic energy loss in KTaO3 crystal *Mater Des* **223** 111248

[9] Zhang Y and Weber W J 2020 Ion irradiation and modification: The role of coupled electronic and nuclear energy dissipation and subsequent nonequilibrium processes in materials *Appl Phys Rev* **7** 041307

[10] Han X, Zarkadoula E, Huang Q, Crespillo M L, Wang X and Liu P 2022 Concentric core-shell tracks and spectroscopic properties of SrTiO3 under intense electronic excitation *Nano Today* **46** 101612

[11] Han X, Zarkadoula E, Crespillo M L, Huang Q, Pan S, Liu C, Zhang M, Wang X and Liu P 2023 Structural Damage and Recrystallization Response of Garnet Crystals to Intense Electronic Excitation (Adv. Funct. Mater. 8/2023) *Adv Funct Mater* **33** 2370045

[12] Velişa G, Wendler E, Wang L-L, Zhang Y and Weber W J 2019 Ion mass dependence of irradiation-induced damage accumulation in KTaO3 *J Mater Sci* **54** 149–58

[13] Meldrum A, Boatner L A and Ewing R C 1998 Effects of ionizing and displacive irradiation on several perovskite-structure oxides *Nucl Instrum Methods Phys Res B* **141** 347–52

[14] Meldrum A, Boatner L A, Weber W J and Ewing R C 2002 Amorphization and recrystallization of the ABO3 oxides *Journal of Nuclear Materials* **300** 242–54

[15] Han X, Liu Y, Huang Q, Crespillo M L, Liu P and Wang X 2020 Swift heavy ion tracks in alkali tantalate crystals: a combined experimental and computational study *J Phys D Appl Phys* **53** 105304

[16] Velişa G, Zarkadoula E, Iancu D, Mihai M D, Grygiel C, Monnet I, Kombaiah B, Zhang Y and Weber W J 2021 Near-surface modification of defective KTaO3 by ionizing ion irradiation *J Phys D Appl Phys* **54** 375302

[17] Waiblinger M, Sommerhalter C, Pietzak B, Krauser J, Mertesacker B, Lux-Steiner M C, Klaumünzer S, Weidinger A, Ronning C and Hofsäß H 1999 Electrically conducting ion tracks in diamond-like carbon films for field emission *Appl Phys A Mater Sci Process* **69** 239–40

[18] Yamaichi E, Watanabe K, Imamiya K and Ohi K 1987 Photoluminescence in KTaO3 Single Crystal *J Physical Soc Japan* **56** 1890–7

[19] Iancu D, Zarkadoula E, Mihai M D, Burducea C, Burducea I, Straticiuc M, Zhang Y, Weber W J and Velişa G 2023 Revealing two-stage phase transition process in defective KTaO3 under inelastic interactions *Scr Mater* **222** 115032

[20] Burducea I, Straticiuc M, Ghiță D G, Moșu D V, Călinescu C I, Podaru N C, Mous D J W, Ursu I and Zamfir N V 2015 A new ion beam facility based on a 3 MV Tandetron^{TM} at IFIN-HH, Romania *Nucl Instrum Methods Phys Res B* **359** 12–9

[21] Velişa G, Andrei R F, Burducea I, Enciu A, Iancu D, Mirea D A, Spiridon A and Straticiuc M 2021 Joint research activities at the 3 MV Tandetron^{TM} from IFIN-HH *The European Physical Journal Plus 2021 136:11* **136** 1–13

[22] Ziegler J F and Biersack J P 1985 The Stopping and Range of Ions in Matter *Treatise on Heavy-Ion Science* (Boston, MA: Springer US) pp 93–129

[23] Zhang Y, Lian J, Zhu Z, Bennett W D, Saraf L V, Rausch J L, Hendricks C A, Ewing R C and Weber W J 2009 Response of strontium titanate to ion and electron irradiation *Journal of Nuclear Materials* **389** 303–10

[24] Jiang W, Devanathan R, Sundgren C J, Ishimaru M, Sato K, Varga T, Manandhar S and Benyagoub A 2013 Ion tracks and microstructures in barium titanate irradiated with swift heavy ions: A combined experimental and computational study *Acta Mater* **61** 7904–16

[25] Nuckols L, Crespillo M L, Xu C, Zarkadoula E, Zhang Y and Weber W J 2020 Coupled effects of electronic and nuclear energy deposition on damage accumulation in ion-irradiated SiC *Acta Mater* **199** 96–106

[26] Zarkadoula E, Jin K, Zhang Y and Weber W J 2017 Synergistic effects of nuclear and electronic energy loss in $KTaO_3$ under ion irradiation *AIP Adv* **7** 015016

[27] Zarkadoula E, Zhang Y and Weber W J 2020 Molecular dynamics simulations of the response of pre-damaged SrTiO3 and KTaO3 to fast heavy ions *AIP Adv* **10** 015019

[28] Waligórski M P R, Hamm R N and Katz R 1986 The radial distribution of dose around the path of a heavy ion in liquid water *Int J Rad Appl Instrum D* **11** 309–19

[29] Bierschenk T, Giulian R, Afra B, Rodriguez M D, Schauries D, Mudie S, Pakarinen O H, Djurabekova F, Nordlund K, Osmani O, Medvedev N, Rethfeld B, Ridgway M C and Kluth P 2013 Latent ion tracks in amorphous silicon *Phys Rev B Condens Matter Mater Phys* **88** 174111

[30] Ridgway M C, Bierschenk T, Giulian R, Afra B, Rodriguez M D, Araujo L L, Byrne A P, Kirby N, Pakarinen O H, Djurabekova F, Nordlund K, Schleberger M, Osmani O, Medvedev N, Rethfeld B and Kluth P 2013 Tracks and voids in amorphous Ge induced by swift heavy-ion irradiation *Phys Rev Lett* **110**

[31] Sachan R, Zarkadoula E, Lang M, Trautmann C, Zhang Y, Chisholm M F and Weber W J 2016 Insights on dramatic radial fluctuations in track formation by energetic ions *Scientific Reports 2016 6:1* **6** 1–7
[32] Aidhy D S, Sachan R, Zarkadoula E, Pakarinen O, Chisholm M F, Zhang Y and Weber W J 2015 Fast ion conductivity in strained defect-fluorite structure created by ion tracks in Gd2Ti2O7 *Scientific Reports 2015 5:1* **5** 1–8
[33] Hanžek J, Fazinić S, Kumar S and Karlušić M 2024 Threshold for ionization-induced defect annealing in silicon carbide *Radiation Physics and Chemistry* **215** 111362
[34] Turos A, Gaca J, Wojcik M, Nowicki L, Ratajczak R, Groetzschel R, Eichhorn F and Schell N 2004 Virtues and pitfalls in structural analysis of compound semiconductors by the complementary use of RBS/channeling and high resolution X-ray diffraction *Nucl Instrum Methods Phys Res B* **219–220** 618–2

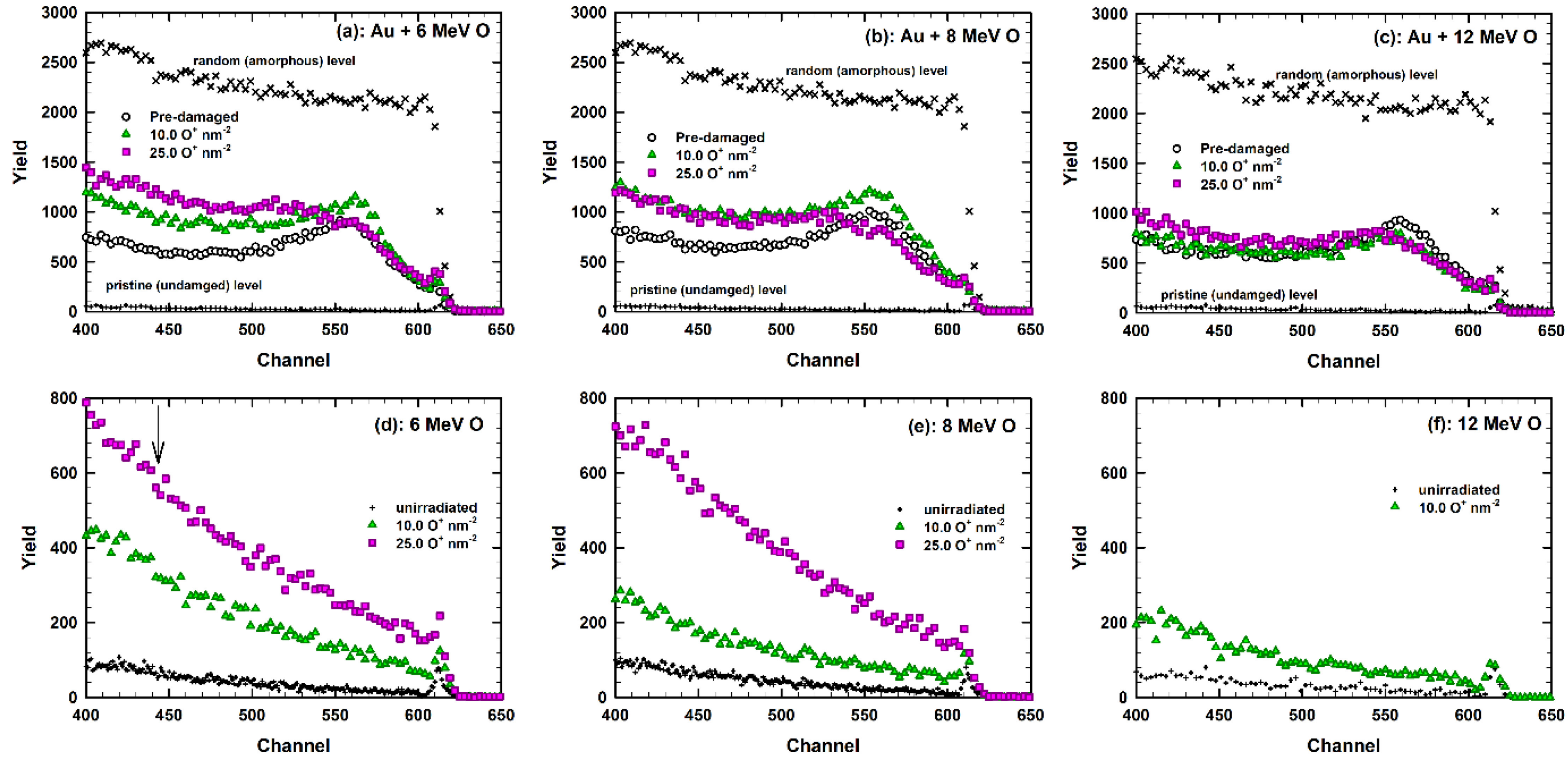

Fig. 1. The RBS/C spectra recorded for pre-damaged and $KTaO_3$ single crystals irradiated at 300 K with (a) 6 M, (b) 8 MeV and (c) 12 MeV O ions at the indicated fluences. For comparison, RBS results for pristine $KTaO_3$ single crystals irradiated at 300 K with (d) 6 MeV (e) 8 MeV and (f) 12 MeV O ions, at the indicated fluences, are also illustrated. Note the RBS spectra recorded in random and channeling direction from a pristine crystal are also shown.

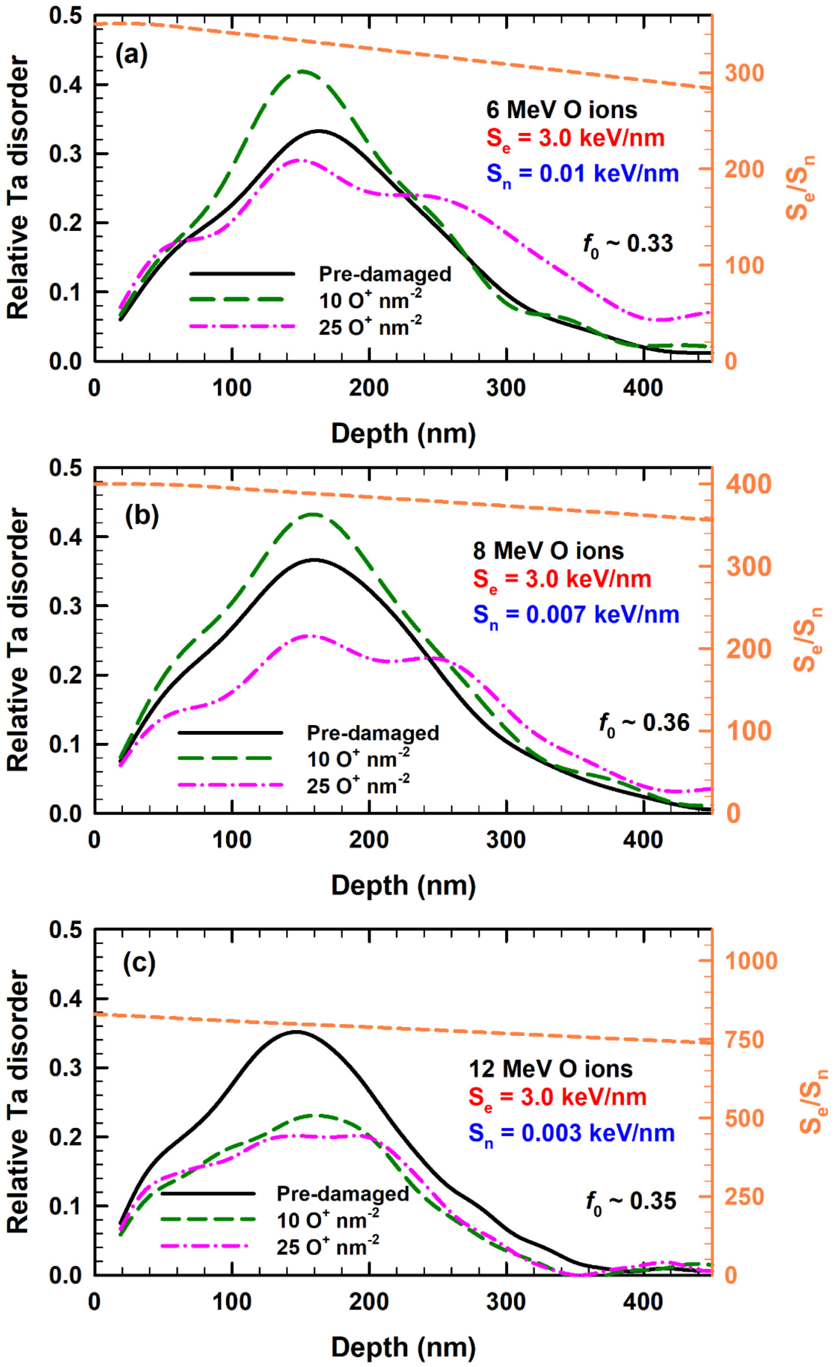

Fig. 2. Relative Ta disorder profiles for pre-damaged $KTaO_3$ single crystals with a maximum initial disorder fraction $f_0 \sim 0.3$ and sequentially irradiated with: (a) 6 MeV O ions, (b) 8 MeV O ions and (c) 12 MeV O ions at the indicated ion fluences. Also superimposed are the SRIM-derived ratio S_e/S_n curves (orange dash-dot lines). The experiment uncertainty is estimated to be ∼15%, which can mainly be attributed to the statistics of the backscattering spectra [32] and to the standard deviation in fitting the experimental disorder profiles.

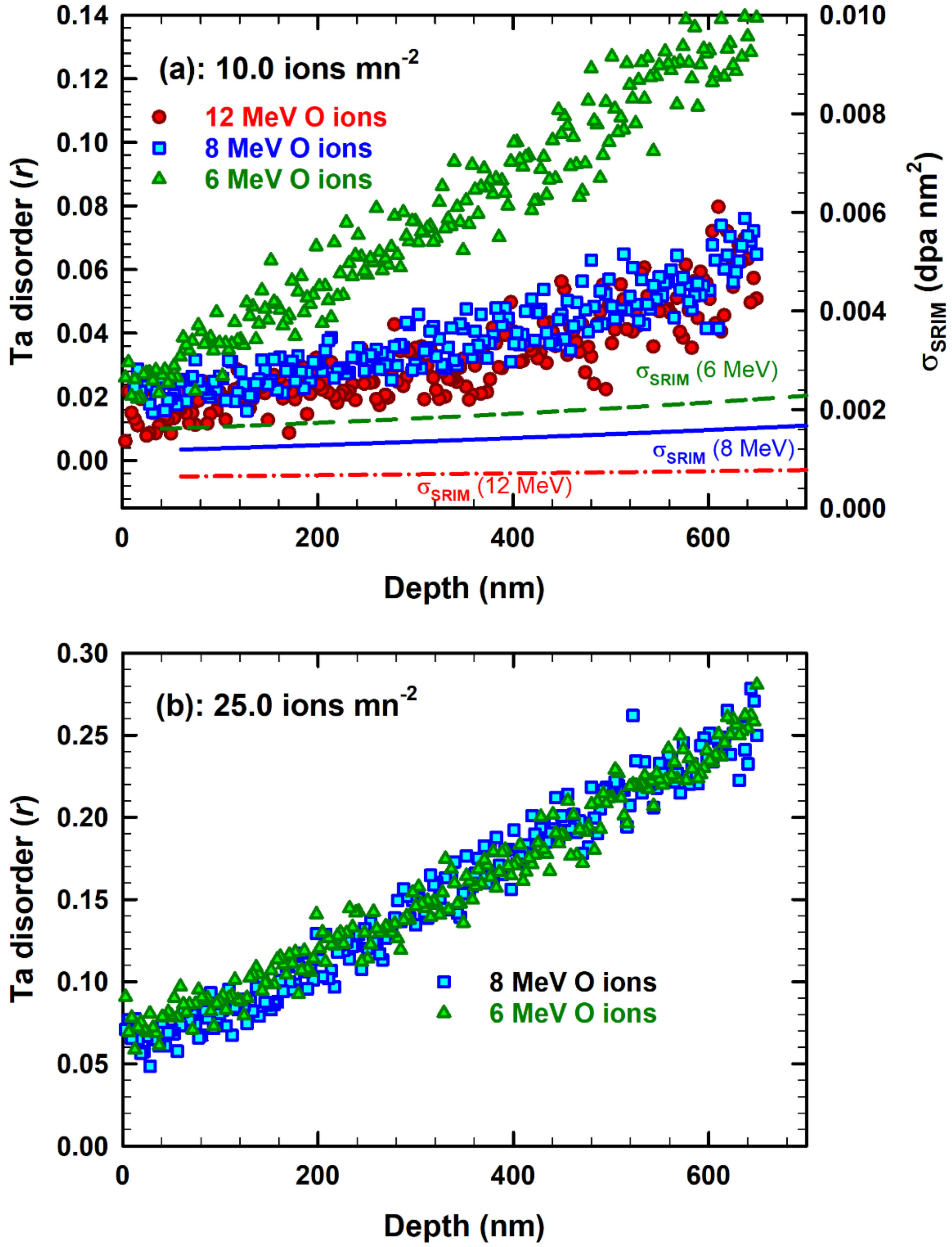

Fig. 3. Disorder on Ta-sublattice as a function of depth for pristine $KTaO_3$ irradiated with 6 MeV (filled triangles), 8 MeV (filles squares) and 12 MeV O (filled circles) ions to ion fluences of (a) 10 ions nm^{-2} and (b) 25 ions nm^{-2}. Also superimposed in Fig. 3 (a) are the displacement cross section (σ_{SRIM}) depth profiles (lines).

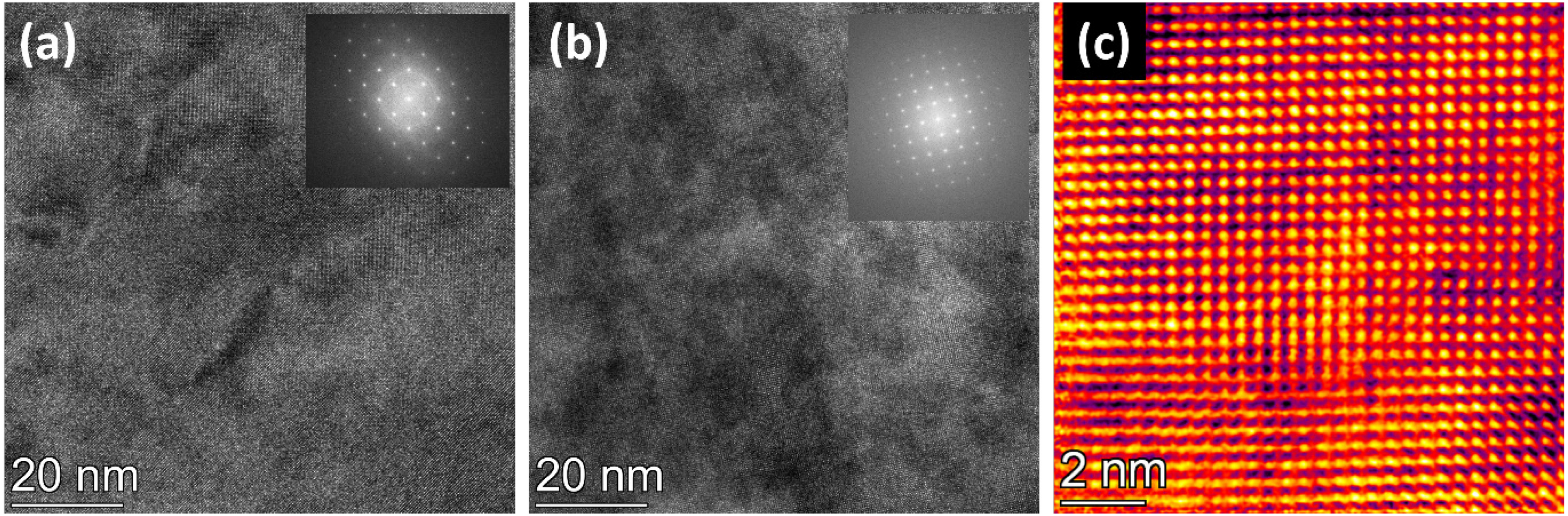

Fig. 4. HRTEM micrographs showing the microstructure changes of the $KTaO_3$ single crystals: (a) pre-damaged with 2.0 MeV Au ions at 300 K to ion fluence of 0.11 ions nm^{-2} and (b) subsequently irradiated with 6 MeV O ions at 300 K to ion fluence of 25.0 ions nm^{-2}. (c) The HAADF image showing the remaining residual damage upon subsequent irradiation with 6 MeV O ions at 300 K to ion fluence of 25.0 ions nm^{-2}. Note that the HRTEM micrographs were recorded at the initial Au-induced damage peak (~160 nm).

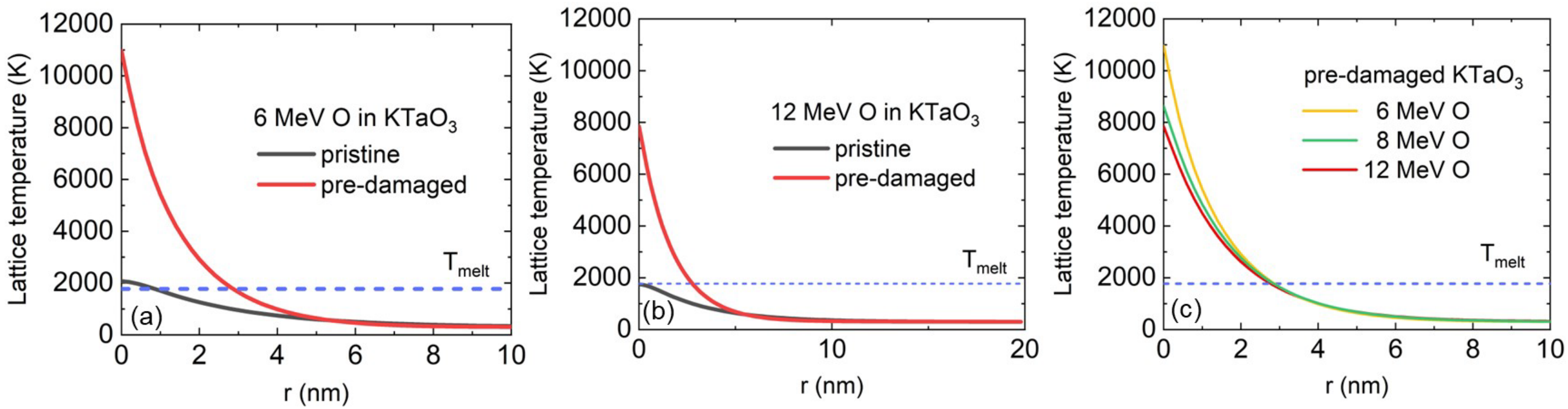

Fig. 5. Comparison between the radial profile of maximum lattice temperature in pristine and pre-damaged $KTaO_3$ containing 30% Frenkel pairs under (a) 6 MeV and (b) 12 MeV O ion irradiation. (c) The radial profile of maximum lattice temperature in pre-damaged $KTaO_3$ containing 30% Frenkel pairs predicted at a time of 30 fs by the inelastic thermal spike calculation for the indicated ion species. The melting temperature (T_M) of pristine $KTaO_3$ is taken from manufacturer data sheet (https://www.alineason.com/).

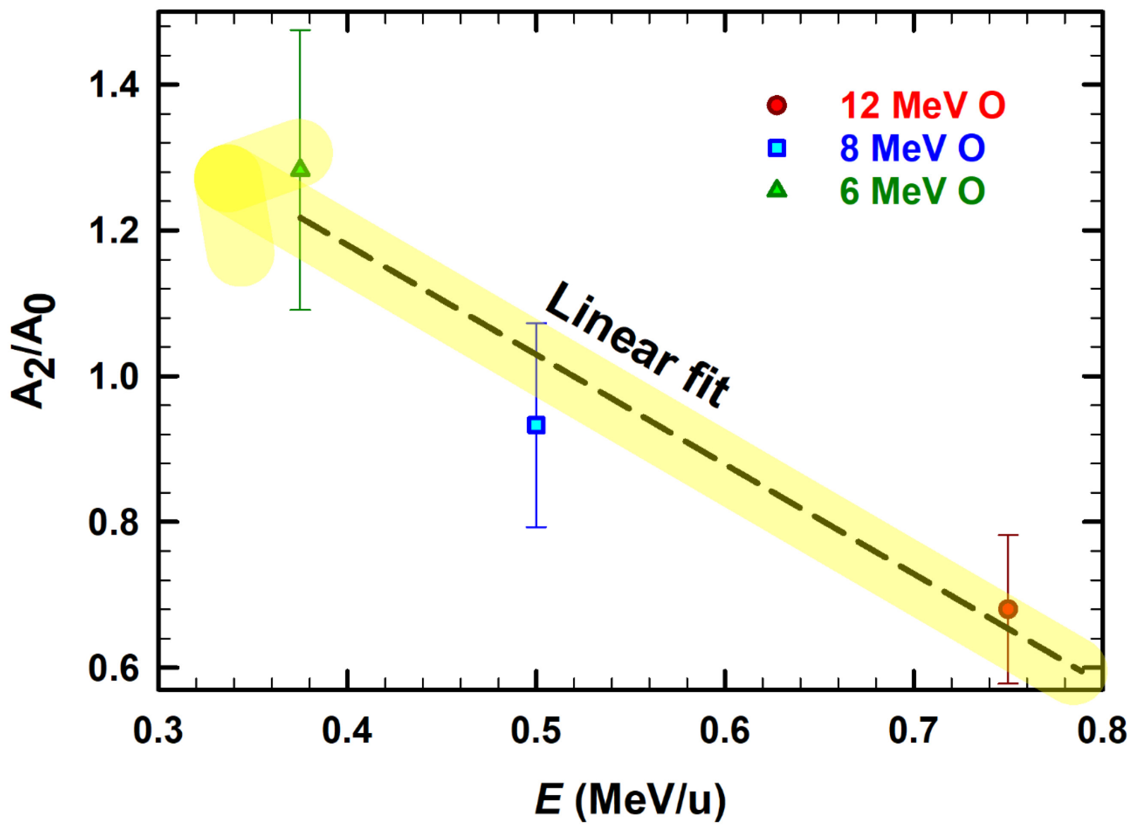

Fig. 6. Relative areal density of damage (A_2/A_0) as a function of specific energy (E). The dash line is linear fit to the data and is only added to guide the eye.